Science Advances
AAAS

advances.sciencemag.org/cgi/content/full/6/42/eaay8892/DC1

Supplementary Materials for

Simulating complex quantum networks with time crystals

M. P. Estarellas*, T. Osada, V. M. Bastidas, B. Renoust, K. Sanaka, W. J. Munro, K. Nemoto

*Corresponding author. Email: mpascualestarellas@gmail.com

Published 16 October 2020, *Sci. Adv.* **6**, eaay8892 (2020)
DOI: 10.1126/sciadv.aay8892

The PDF file includes:

Other Supplementary Material for this manuscript includes the following:

(available at advances.sciencemag.org/cgi/content/full/6/42/eaay8892/DC1)

Movie S1

I. A ROADMAP THROUGH THE SUPPLEMENTARY MATERIALS

The purpose of this supplementary material is to provide the reader with the necessary tools to understand the main manuscript. In section II we focus on the relation between the robustness of time crystals and many-body localization (MBL). We explain in detail how to obtain the level statistics for the quasienergy gaps, which is a well-known diagnostic of MBL. In section III we show how to obtain signatures of the melting process by calculating the power spectrum of a time series of measured observables. Our approach is experimentally feasible and provides clear evidence that some configurations are more stable than others. In section IV we provide a semiclassical description of the stability of the different spin configurations. Finally, a very important aspect of our results is that there is an emergent scale-free behavior in the graphs associated to the DTC. With this purpose in mind, in section V we provide an experimental protocol to simulate complex quantum networks in near-term quantum devices. Our approach is based on a quantum walk in the configuration space, which can be realized by measuring l-point spin correlation functions.

II. LEVEL STATISTICS OF THE QUASIENERGIES AND MANYBODY LOCALIZATION

In classical mechanics, integrable systems are characterized by the existence of integrals of motion restricting the motion to orbits that are constrained by conservation rules. The classical harmonic oscillator, for example, exhibits a two-dimensional phase space with coordinates q and p representing position and momentum, respectively. In the absence of driving, the energy of the oscillator is conserved. Thereby, given an initial condition (q_0, p_0), the classical orbits are constrained to the energy surface $E(q,p) = p^2/2M + M\Omega q^2/2 = p_0^2/2M + M\Omega q_0^2/2$, where M is the mass and Ω is the oscillation frequency of the oscillator. For any value of the energy, the classical orbits are periodic with a period $T_{\text{orbit}} = 2\pi/\Omega$. In the quantum world, quantum signatures of the periodic orbits appear in the spacings $\delta_n = E_{n+1} - E_n = \hbar\Omega$ between the eigenvalues $E_n = \hbar\Omega(n-1/2)$ of the Hamiltonian $\hat{H} = \hbar\Omega(\hat{a}^\dagger\hat{a} - 1/2)$, with n labelling each of the system's eigenstates and $\hat{a}$ ($\hat{a}^\dagger$) being the anhiliation (creation) operator. Interestingly, if we calculate the probability distribution of level spacings δ_n, this would be a Dirac delta distribution centered at Ω. When we break conservation rules, however, the integrability of the system is compromised because the conserved quantities are destroyed and the level spacing distribution largely deviates from a simple Dirac-delta type distribution. This statistical

---

* These authors contributed equally.

analysis is one of the cornerstones of recent developments in the theory of thermalization, which is closely related to random matrix theory and quantum signatures of chaos [36, 37].

Recently, there has been an increasing interest in the study of level statistics as a diagnosis for thermalization and manybody localization. In the context of quantum manybody systems, the interactions distribute the energy between all the available states, because they usually break conserved quantities at the single-particle level, leading to thermalization and ergodic behavior. In systems where there is a well defined semiclassical limit, this behavior is associated with a fully chaotic phase space [36, 37]. As we discussed above, in quantum mechanics, level statistics is a powerful tool to determine the nature of the dynamics. In terms of level statistics, this means that the statistical behavior of an ergodic system will largely deviate from the quantum harmonic oscillator case described above. In particular, the destruction of conserved quantities induces strong correlations between the energy eigenvalues that are reflected in a strong level repulsion [37]. In the case of disordered manybody systems, there is a competition between disorder and interactions. Disorder can suppress ergodicity giving rise to the manybody localized phase, which is characterized by an extensive number of conserved quantities [38–40]. In the absence of drive, one is interested in the distribution of ratios $P(r)$ with $r_s = \min(\delta_s, \delta_{s+1})/\max(\delta_s, \delta_{s+1}) \leq 1.0$ with $\delta_s = E_{s+1} - E_s$, where E_s are the energy eigenvalues sorted in order of increasing value [37]. In the MBL phase, the levels are uncorrelated because the manybody states are highly localized in space and the level statistics follows a Poissonian distribution

$$P_{\text{Poisson}}(r) = \frac{2}{(1+r)^2}\,. \tag{S1}$$

When the interactions overcome the effect of disorder, the aforementioned conserved quantities are destroyed and the system is able to explore all the configuration space with a constant energy. This is reflected in a strong level repulsion because some states are delocalized. As a consequence, in the case of real Hamiltonians, the system follows a universal level statistics

$$P_{\text{GOE}}(r) = \frac{27}{4}\frac{r + r^2}{(1 + r + r^2)^{5/2}} \tag{S2}$$

associated to the Gaussian Orthogonal ensemble (GOE) of random matrices [37, 41].

In our manuscript, we are interested in the dynamics of DTCs under the effect of a rotation error as shown in the Hamiltonian from Eq. (1). Below we show that the time-crystalline order is directly related to the presence of an MBL phase. In analogy to the quantum harmonic oscillator, in the absence of error, the time crystal has several conserved quantities and the motion is periodic. However, discrete time crystals are quantum phases of matter that appear in periodically-driven quantum systems and energy is not conserved anymore. Therefore, we have to work with gaps $\delta_s = \lambda_{s+1} - \lambda_s$, where $-\hbar\omega/2 < \lambda_s < \hbar\omega/2$ are the quasienergies and ω is the frequency of the drive. Under the effect of a small rotation error, there is a small coupling between different symmetry multiplets and the quasienergy level statistics follows a Poissonian behavior as in Eq. (S1). As a consequence, the system is in the MBL phase, which protects the system from heating up to infinite temperatures [9, 42]. When the error is increased, the conserved quantities are destroyed and the Floquet states become highly delocalized in the configuration space. The DTC melts and an MBL-to-ergodic phase transition takes place. The statistics of levels in this case is given by

$$P_{\text{COE}}(r) = \frac{2}{3}\left\{\left[\frac{\sin\left(\frac{2\pi r}{r+1}\right)}{2\pi r^2}\right] + \frac{1}{(1+r)^2} + \left[\frac{\sin\left(\frac{2\pi}{r+1}\right)}{2\pi}\right]\right\} - \frac{2}{3}\left\{\left[\frac{\cos\left(\frac{2\pi}{r+1}\right)}{2\pi r^2}\right] + \left[\frac{\cos\left(\frac{2\pi r}{r+1}\right)}{r(r+1)}\right]\right\} \tag{S3}$$

which is the same statistics as the circular orthogonal ensemble of random matrices [42, 43].

One of the most intriguing aspects of level statistics is its intimate relation to quantum signatures of chaos and random matrix theory. At this stage, it is important to clarify a technical point concerning the transition between regular and chaotic motion and its intimate relation to the MBL-to-ergodic transition in manybody systems. As we discussed above, the MBL phase is characterized by an extensive number of conserved quantities, which leads to a Poissonian level statistics. Under the effect of a perturbation, these conserved quantities are destroyed and the system has a transition to the ergodic phase. This process resembles the destruction of tori in phase space within the framework of KAM theorem. For small perturbations, some tori are more susceptible to be destroyed and as we increase the strength of the perturbation, the phase space becomes mixed: there are regular islands associated to the surviving tori and a chaotic sea. When all the tori are destroyed, the dynamics is fully chaotic. In quantum systems, signatures of this chaotic dynamics lead to a universal behavior of the level statistics giving rise to distributions $P_{\text{GOE}}(r)$ and $P_{\text{COE}}(r)$ for undriven and driven systems, respectively. Universality means that these distributions do not depend on microscopic details of the dynamics but are solely determined by symmetries of the system. However, quantum signatures of a mixed phase space are not universal. In the context of time crystals, when we increase the error, we see a crossover between $P_{\text{Poisson}}(r)$ and $P_{\text{COE}}(r)$, because the error destroys conserved quantities. As we increase the rotation error, we observe that the level statistics is closer to $P_{\text{COE}}(r)$. Figure S1 depicts the results for the level statistics in the case of a time crystal for errors $\epsilon = 0.01$ and $\epsilon = 0.1$. Our results therefore show that time crystalline order is protected by MBL.

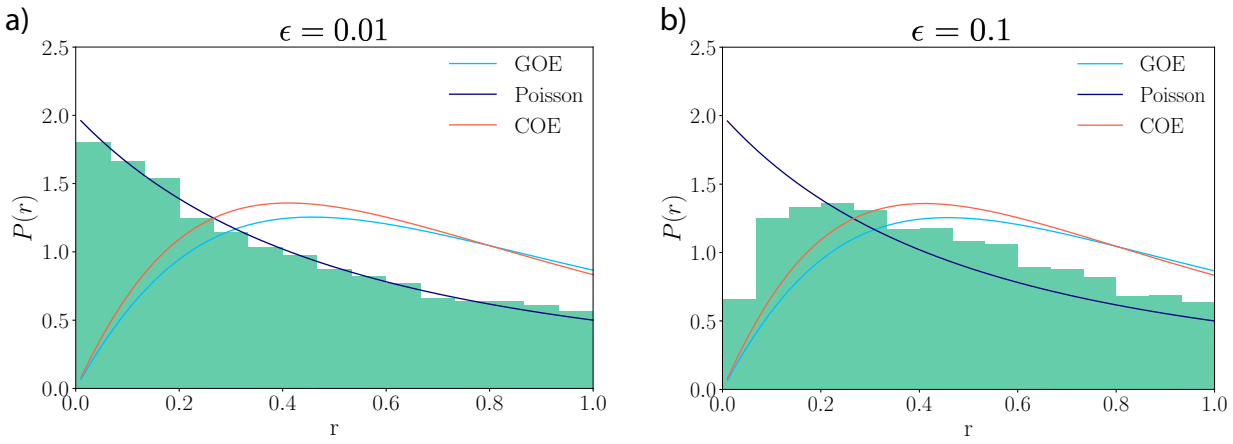

Figure S1. Statistical analysis of the ratios $r_\alpha = \min(\delta_s, \delta_{s+1})/\max(\delta_s, \delta_{s+1})$ between quasienergy gaps $\delta_s = \lambda_{s+1} - \lambda_s$. To obtain enough data, we calculate the quasienergy spectrum of a spin chain with $n = 8$ sites for 50 realizations of disorder. a) For a small value $\epsilon = 0.01$ of the rotation error, the levels are uncorrelated and the statistical behavior resembles a Poissonian distribution, which is a signature of MBL phase. b) By increasing the error to $\epsilon = 0.1$, the statistics is closer to the circular orthogonal ensemble. As long as the system remains in the MBL phase, the time-crystalline order can still be obserevd. We considered the same parameters used in the main text.

III. POWER SPECTRUM OF TIME SERIES: STABILITY OF THE TIME-CRYSTALLINE PHASE

In this section our aim is to provide an additional experimentally-accessible way to investigate the stability of the different configurations. The latter will shed light on the melting mechanism of the time crystal and the emergent scale-free behavior. Our idea is based on a quantity that can be easily measured in several platforms. We just require to measure the expectation value of the total magnetization $M_{i,Z}(mT) = 1/n \sum_{r=1}^{n} \langle\psi(mT)|\sigma_r^z|\psi(mT)\rangle$ at stroboscopic times, where $|\psi(0)\rangle = |i\rangle$. This quantity is related to the populations, as follows

$$M_{i,Z}(mT) = -\frac{1}{n}\sum_{r=1}^{n}\sum_{j=1}^{2^n}(-1)^{j_r}|A_j(mT)|^2 \,, \tag{S4}$$

where $(j_1, j_2, \ldots, j_n)_2$ is the binary decomposition of the integer number j for all the configurations.

Next, for a given initial configuration i, one can record the measurements $M_{i,Z}(mT)$, thus obtaining a time series

$$\{M_{i,Z}(0), M_{i,Z}(T), \ldots, M_{i,Z}(NT)\} \,, \tag{S5}$$

where N is the number of periods that the system evolve. With the data for the time series at hand, we can calculate the discrete Fourier transformation

$$\mathcal{M}_{i,Z}(k) = \frac{1}{N}\sum_{m=1}^{N} e^{-\frac{\mathrm{i}2\pi k}{N}m} M_{i,Z}(mT) = \frac{1}{N}\sum_{m=1}^{N} e^{-\mathrm{i}\omega_k mT} M_{i,Z}(mT) \,, \tag{S6}$$

where $\omega_k = 2\pi k/NT$ and $k \in [0, N-1]$. For a given rotation error ϵ, the associated power spectrum

$$\boldsymbol{V}_{i,\epsilon} = \{|\mathcal{M}_{i,Z}(0)|^2, |\mathcal{M}_{i,Z}(1)|^2 \ldots, |\mathcal{M}_{i,Z}(N-1)|^2\} \tag{S7}$$

tell us how strong is the contribution of a the $k-$th harmonic to the time series. Note that for convenience, we have arranged the Fourier coefficients in the form of a vector $\boldsymbol{V}_{i,\epsilon}$. In the absence of error, all the configurations show a magnetization that varies as $M_{i,Z}(mT) = (-1)^m M_{i,Z}(0) = e^{\mathrm{i}n\pi} M_{i,Z}(0)$ and the power spectrum shows a single peak at a frequency $\omega_{N/2}$, which is half the frequency of the drive. The latter is a signature of the subharmonic response of the manybody system. As we discussed in Sec.II, the periodic motion is related to local integrals of motion. The DTC is protected agains heating due to MBL. However, as we increase the rotation error ϵ, some configurations are more affected than others and they loose their periodic character. On the contrary, configurations like $|2^n - 1\rangle = |\uparrow\uparrow\uparrow \ \ldots \uparrow\uparrow\rangle$ and $|0\rangle = |\downarrow\downarrow\downarrow \ \ldots \downarrow\downarrow\rangle$ are the most stable ones. To have a quantitative measurement of this statement that can be easily accessed in experiments, we propose to measure the fidelity $F_i^{\mathrm{ps}}(\epsilon)$ of the power

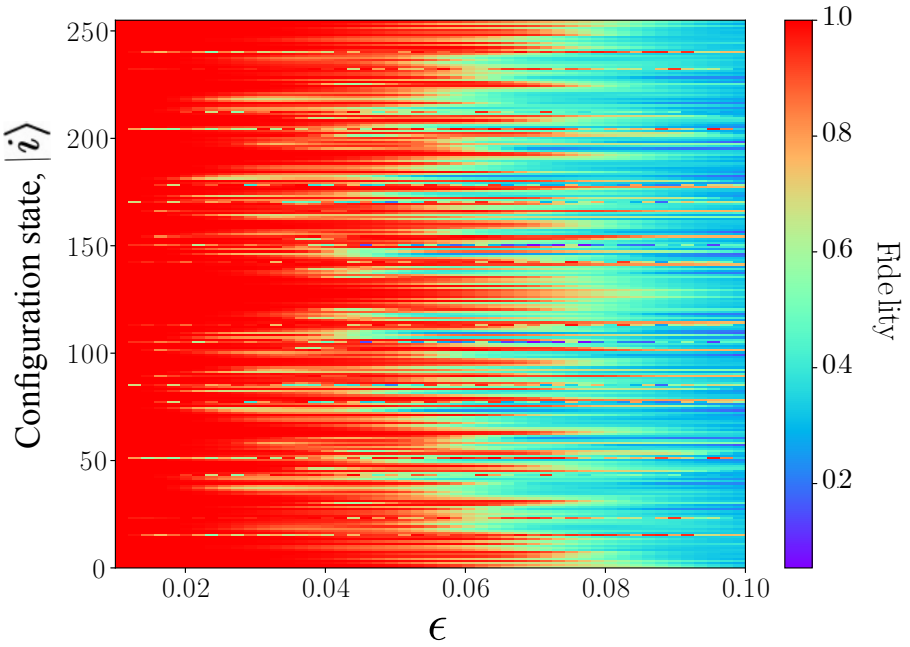

Figure S2. Stability of the different 2^8 configuration states. To investigate the effect of the rotation error on the different configurations $|i\rangle$, we calculate the fidelity $F_i^{\rm ps}(\epsilon)$. The latter is a measure of the periodicity of the dynamics. Our results show that configurations such as $|2^n-1\rangle = |\uparrow\uparrow\uparrow \ \ldots \uparrow\uparrow\rangle$ are more stable under the effect of error. Others, on the contrary, are strongly affected by the rotation error. We consider a time crystal with $n = 8$ sites (256 configurations) and the same parameters used in the main text.

spectrum, defined as follows

$$F_i^{\rm ps}(\epsilon) = \sqrt{\frac{\boldsymbol{V}_{i,0}\cdot\boldsymbol{V}_{i,\epsilon}}{\|\boldsymbol{V}_{i,0}\|\,\|\boldsymbol{V}_{i,\epsilon}\|}}\,. \tag{S8}$$

This very simple quantity tell us how far is the power spectrum from the one of a time crystal without error. In figure S2 we depict the fidelity as a function of the configuration number i and the error ϵ. This shows a clear evidence that not all the configurations are stable under the effect of a rotation error.

IV. SEMICLASSICAL DESCRIPTION OF A DISCRETE TIME CRYSTAL: A STABILITY ANALYSIS OF THE FIXED POINTS IN THE ABSENCE OF ERROR $\epsilon = 0$

In this section, we present numerical evidence of the stability of the different configurations from a semiclassical perspective. We start by considering the effective Hamiltonian for two periods of the drive

$$\hat{H}^{\rm eff}_{\epsilon,2T} = \frac{\hbar T_2}{T}\sum_{lm} J^z_{lm}\sigma^z_l\sigma^z_m - \frac{\hbar g\epsilon T_1}{2T}\sum_l[(\cos(B_l 2T_2)+1)\sigma^x_l + \sin(B_l 2T_2)\sigma^y_l]\,, \tag{S9}$$

which describes the dynamics of the system at stroboscopic times $t_n = 2nT$.

After visualizing the classical orbits on the Bloch sphere, it is instructive to investigate a limiting case of the system. Here we focus on the system in the absence of error. In this case, there is an exact mapping of Eq.(7) to classical Hamiltonian

$$\mathcal{H}_{0,2T}(\theta_1,\ldots,\theta_n) = \frac{\hbar T_2}{T}\sum_{l,m} J^z_{l,m}\cos\theta_l\cos\theta_m\,. \tag{S10}$$

Configurations such as $\theta^c_l = 0,\pi$ are fixed points of the stroboscopic dynamics. The latter can be derived from the first derivative

of the energy function $\partial_{\theta_j}\mathcal{H}_{0,2T}(\theta_1,\ldots,\theta_n)=0$. For example, the quantum $|2^n-1\rangle=|\uparrow\uparrow\uparrow\ \ldots\uparrow\uparrow\rangle$ has a classical counterpart $(\theta_1^c,\theta_2^c,\ldots,\theta_n^c)=(0,0,\ldots,0)$. Given a fixed point, we can explore its stability properties by investigating the eigenvalues of the Jacobian matrix with elements $\mathcal{J}_{i,j}=\partial_{\theta_i}\partial_{\theta_j}\mathcal{H}_{0,2T}(\theta_1,\ldots,\theta_n)|_{\theta=\theta^c}$, where the derivatives are evaluated at the critical points θ^c such that $\partial_{\theta_j}\mathcal{H}_{0,2T}(\theta_1,\ldots,\theta_n)=0$. For simplicity, let us focus on a particular example of a lattice with four sites and open boundary conditions. In the case of the configuration $(\theta_1^c,\theta_2^c,\theta_3^c,\theta_4^c)=(0,0,0,0)$ these matrix elements are given by

$$\begin{aligned}\mathcal{J}_{i,i}&=-\sum_m J^z_{i,m}\cos\theta_i\cos\theta_m|_{\theta=\theta^c}=-\sum_m J^z_{i,m}\\ \mathcal{J}_{i,j}&=J^z_{i,j}\sin\theta_i\sin\theta_j|_{\theta=\theta^c}=0\ .\end{aligned}\tag{S11}$$

and the equilibrium is stable [44]. For any configuration of the form $\theta_l^c=0,\pi$ the off-diagonal elements of the Jacobian matrix are zero. Let us consider the configuration $(\theta_1^c,\theta_2^c,\theta_3^c,\theta_4^c)=(0,0,\pi,\pi\ )$ with one domain wall, where $\mathcal{J}_{1,1}=-J^z_{1,2}+J^z_{1,3}+J^z_{1,4}$, $\mathcal{J}_{2,2}=-J^z_{1,2}+J^z_{2,3}+J^z_{2,4}$, $\mathcal{J}_{3,3}=-J^z_{1,3}+J^z_{2,3}-J^z_{3,4}$ and $\mathcal{J}_{4,4}=J^z_{1,4}+J^z_{2,4}-J^z_{3,4}$. Due to the power-law decay of the couplings, all the diagonal elements are negative and the fixed point is stable. Finally, for a configuration with three domain walls $(\theta_1^c,\theta_2^c,\theta_3^c,\theta_4^c)=(0,\pi,\ 0,\pi)$, the matrix elements are $\mathcal{J}_{1,1}=J^z_{1,2}-J^z_{1,3}+J^z_{1,4}$, $\mathcal{J}_{2,2}=J^z_{1,2}+J^z_{2,3}-J^z_{2,4}$, $\mathcal{J}_{3,3}=-J^z_{1,3}+J^z_{2,3}+J^z_{3,4}$ and $\mathcal{J}_{4,4}=J^z_{1,4}-J^z_{2,4}+J^z_{3,4}$. In this case all the eigenvalues are positive. The elements of the Jacobian give us information about the local curvature of the energy function at the critical points. As long as they have the same sign, the fixed points are stable. For a non-zero value of the error, configurations such as $\theta_l^c=0,\pi$ are not fixed points of the dynamics anymore, but they belong to trajectories in phase space.

V. QUANTUM WALKS IN THE CONFIGURATIONS SPACE: EXPERIMENTAL PROTOCOL TO SIMULATE COMPLEX QUANTUM NETWORKS

So far, we have discussed spectral properties of driven systems and its consequences for the time crystal. The percolation rule discussed in the main text provides us with graphical way to represent localization properties of Floquet states. Therefore, the connectivity of the graph tell us information about how many configurations "participate" in a given Floquet state. When the latter are delocalized, the gaps between quasienergies become highly correlated and the system becomes ergodic as we discussed in section II. This establish an intriguing relation between the melting of a discrete time crystal and the MBL-to-ergodic transition as we increase the rotation error. During this process, the graph exhibits a scale-free behavior characteristic of complex quantum networks. Here, we describe in detail an experimental protocol to faithfully extract structural information about the simulated complex quantum networks in Noisy intermediate-scale quantum devices.

The cornerstone of our approach is the representation of the effective Hamiltonian

$$\hat{H}^{\rm eff}_{\epsilon,T}=\sum_i\mathcal{E}_i|i\rangle\langle i|+\sum_{i,j}K_{ij}|i\rangle\langle j|=\sum_s\lambda_s|\Phi_s\rangle\langle\Phi_s|\tag{S12}$$

in terms of the configuration basis states $\{|i\rangle\}$. Here $\mathcal{E}_i$ is the energy of configuration $|i\rangle$, and K_{ij} is the transition energy between configurations $|i\rangle$ and $|j\rangle$. The quasienergies λ_s have a complicated dependence on the parameters $\mathcal{E}_i$ and K_{ij} that determine localization properties of the Floquet states $|\Phi_s\rangle$. The latter are linear combinations of configurations $|i\rangle$ with $i=0,1,2\ldots,2^n-1$, where n is the number of sites of the spin chain. Interestingly, although the effective Hamiltonian describes a manybody system, in terms of configurations, the dynamics resemble a quantum walk in a quantum complex network.

Experimentally, one can initially prepare the state of the system in a given configuration such as $|\psi(0)\rangle=|i\rangle=|\uparrow\uparrow\uparrow\ \ldots\downarrow\downarrow\rangle$, which represents a node of the complex network. At stroboscopic times $t_n=nT$, the dynamics are governed by the effective Hamiltonian $\hat{H}^{\rm eff}_{\epsilon,T}$ and the evolution of the state reads $|\psi(nT)\rangle=e^{-i\hat{H}^{\rm eff}_{\epsilon,T}nT/\hbar}|\psi(0)$. Inherently, the most relevant aspects of the dynamics can be recovered from this discrete evolution. Next, let us focus on the density matrix

$$\hat{\rho}(nT)=|\psi(nT)\rangle\langle\psi(nT)|=\sum_{i,j}A_i(nT)A_j^*(nT)|i\rangle\langle j|,\tag{S13}$$

where $|\psi(nT)\rangle=\sum_i A_i(nT)||i\rangle$. This expression give us already a recipe to measure the dynamics of the quantum walk in existing Noisy intermediate-scale quantum devices. This requires a modest set of measurements and it is straightforward with current experimental feasibilities. The idea is to measure the populations $\rho_{i,i}(nT)=|A_i(nT)|^2$ of the density matrix stroboscopically, to determine which configurations are occupied. This information can be accessed by measuring the correlation functions

$$C_{i,Z}(nT) = \mathrm{tr}\left[\hat{\rho}(nT)|i\rangle\langle i|\right] = |A_i(nT)|^2$$
$$= \frac{1}{2^n}\mathrm{tr}\left[\hat{\rho}(nT)(\sigma_1^z - (-1)^{i_1}\hat{I})(\sigma_2^z - (-1)^{i_2}\hat{I})\cdots(\sigma_n^z - (-1)^{i_n}\hat{I})\right] , \tag{S14}$$

corresponding to all the configurations $i = 0, 1, 2, \ldots, 2^n - 1$. Here $(i_1, i_2, \ldots, i_n)_2$ is the binary decomposition of the integer number i. For example, if we want to measure the population of the configuration $|2^n - 1\rangle = |\uparrow\uparrow\uparrow \ \ldots \uparrow\uparrow\rangle$, we need to measure the correlation

$$C_{2^{n-1},Z}(nT) = \frac{1}{2^n}\mathrm{tr}\left[\hat{\rho}(nT)(\sigma_1^z + \hat{I})(\sigma_2^z + \hat{I})\cdots(\sigma_n^z + \hat{I})\right] , \tag{S15}$$

because $2^{n-1} = (1, 1, \ldots, 1)_2$. Similarly, to measure the population of $|0\rangle = |\downarrow\downarrow\downarrow \ \ldots \downarrow\downarrow\rangle$, we need to measure the correlation

$$C_{0,Z}(nT) = \frac{1}{2^n}\mathrm{tr}\left[\hat{\rho}(nT)(\sigma_1^z - \hat{I})(\sigma_2^z - \hat{I})\cdots(\sigma_n^z - \hat{I})\right] , \tag{S16}$$

as $0 = (0, 0, \ldots, 0)_2$. Interestingly, the aforementioned correlations can be reconstructed from measurements of all the possible combinations of single-point correlators $C_Z^{r_1}(nT) = \mathrm{tr}\left[\hat{\rho}(nT)\sigma_{r_1}^z\right]$, two-point correlators $C_Z^{r_1,r_2}(nT) = \mathrm{tr}\left[\hat{\rho}(nT)\sigma_{r_1}^z\sigma_{r_2}^z\right]$ up to n-point correlators $C_Z^{r_1,r_2,\ldots,r_n}(nT) = \mathrm{tr}\left[\hat{\rho}(nT)\sigma_{r_1}^z\sigma_{r_2}^z\cdots\sigma_{r_n}^z\right]$. In trapped ions, it is possible to measure these correlations by resorting to measurements on single ions. In superconducting qubits, it is even possible to perform full tomography for qubits arrays up to $N = 12$ qubits and measurements of these correlations are within reach with current technology [45]. After recording the data of the populations $|A_i(nT)|^2$ for all the configurations i at stroboscopic times $t_n = nT$, one can generate a space-time plot to depict the data $[nT, i, \rho_{i,i}(nT)]$. The latter is depicted in Fig. S3. The color scale represent the populations and one can visualize how the initial states travel through the configuration space.

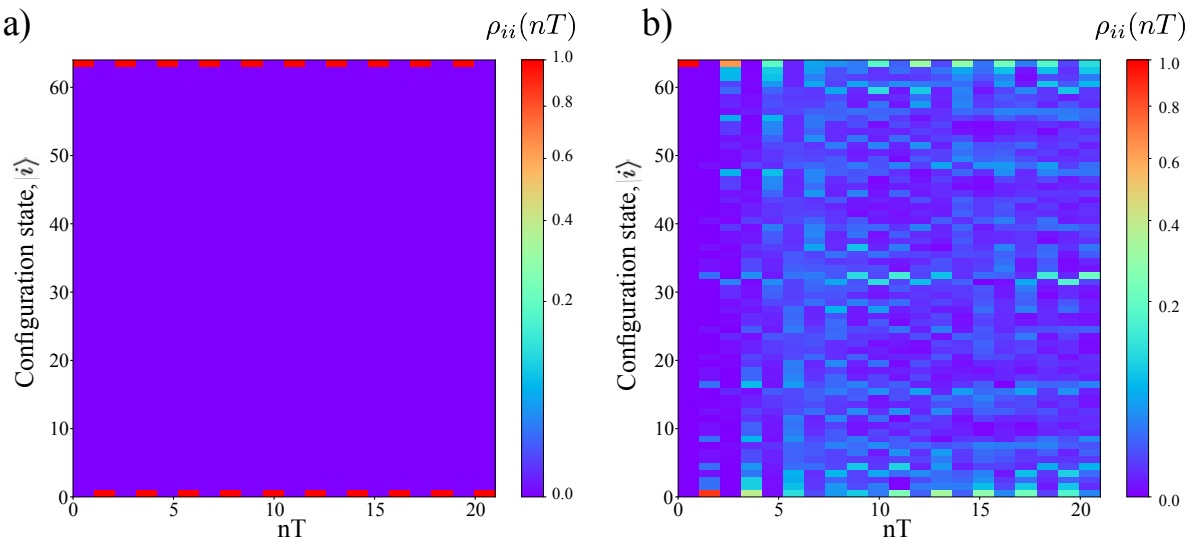

Figure S3. Quantum simulation of a complex quantum network of $n = 6$ sites. One of the cornerstone of our work is the possibility to use time crystals as a quantum simulator for a complex quantum network. In terms of the configurations $|i\rangle$, the effective Hamiltonian S12 is a tight binding model on a complex quantum network. To experimentally simulate the dynamics of an excitation in such a network, one can prepare a configuration $|\psi(0)\rangle = |i\rangle$ as the initial state of the system. For example, we can prepare $|\psi(0)\rangle = |2^n - 1\rangle = |\uparrow\uparrow\uparrow \ \ldots \uparrow\uparrow\rangle$ and register the stroboscopic evolution of the populations $\rho_{i,i}(nT)$ of the different configurations $|i\rangle$ at stroboscopic times $t_n = nT$. a) Depicts the evolution of the populations in the absence of error $\epsilon = 0$. In this case, the network is composed by a set of decoupled dimers. Therefore, the dynamics takes place between two configurations $|0\rangle$ and $|2^n - 1\rangle$. b) Shows the dynamics of the populations for an error $\epsilon = 0.1$. For this value of the error, the complex network exhibits clusters and the system can populate more configurations in the Hilbert space. We consider a time crystal with $n = 6$ sites (64 configurations) and the same parameters used in the main text.

The experimental protocol mentioned above provides us with a way of accessing very relevant information related to its degree distribution. To have a simple picture of this idea in mind, let us consider the case of a DTC in the absence of rotation error. In this case, if we prepare an initial configuration $|\psi(0)\rangle = |\uparrow\uparrow\uparrow \ \ldots \downarrow\downarrow\rangle$, this correspond to a Floquet cat state, because it is a

quantum superposition of two Floquet states with quasienergies $\pm\hbar\pi/T$. Therefore, the expectation value of the total transverse magnetization $M_{i,Z}(nT) = 1/n \sum_{r=1}^{n} \langle\psi(nT)|\sigma_r^z|\psi(nT)\rangle$ will show an oscillatory behavior with a period $2T$. In the configuration space, the quantum walk will show dynamics between just two configurations $|2^n - 1\rangle = |\uparrow\uparrow\uparrow \ \ldots \uparrow\uparrow\rangle$ and $|0\rangle = |\downarrow\downarrow\downarrow \ \ldots \downarrow\downarrow\rangle$. If we now calculate how many configurations "participate" in the quantum state $|\psi(nT)\rangle$, then we have a measure of how connected the network in the configuration space is. To be more precise, let us define the participation ratio

$$P_i(nT) = \frac{1}{\sum_{i=1}^{2^n} |A_i(nT)|^4} , \tag{S17}$$

which can be obtained from the measurement of the correlation function Eq. (S14).

When approximating $\hat{H}^{\text{eff}}_{\epsilon,T}$ up to a first order in the error ϵ, one can easily see that the local rotation that connects different resonant configurations (and therefore generates the clusters in the graph) has an approximate tunneling time of $\tau \sim \frac{T}{g\epsilon T_1}$. If we obtain $P_i(\tau)$ for a given initial i-th node or configuration, one can estimate how many configurations have been visited after the evolution time τ, and thus estimate the degree of this node. If we now repeat the process for all the possible initial configurations $i = 0, 1, 2, \ldots, 2^n - 1$ one can obtain a distribution for the participation ratio, PR. In Fig. S4 we present the distributions obtained from this experimental protocol for the same system that was depicted in Fig. 2 (network of $n = 8$ sites and a rotation error of $\epsilon = 0.012$ and $\epsilon = 0.1$). We note that the shape of the distributions obtained from the calculation of $P_i(\tau)$, **a)** heavy-tailed with a power-law fit and **b)** normal distribution, matches the ones of Fig. 2 obtained directly from the degree distribution of the network. In a nutshell, by measuring the aforementioned correlation functions, we can simulate the network and obtain important information without calculating the unitary operator and without full quantum process tomography.

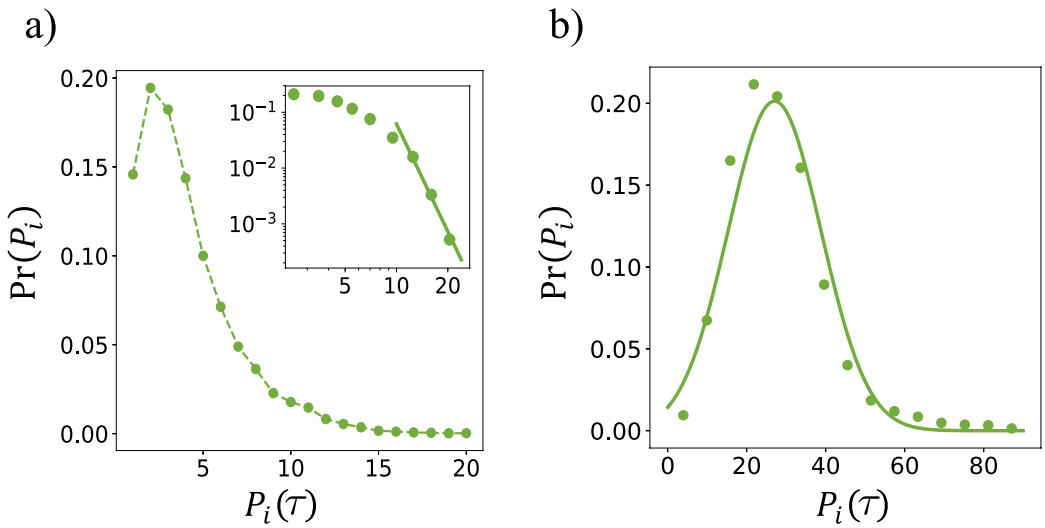

Figure S4. *PT* distributions of a quantum network of $n = 8$ sites as an approximation of the degree distribution of the network using only experimentally accessible data. Information regarding the complexity of the network can be gathered experimentally by the measurement of the correlation function of Eq. S15 and the calculation of the participation ratio, $P_i(\tau)$, at time $\tau \sim \frac{T}{g\epsilon T_1}$ for all the possible initial configurations $i = 0, 1, 2, \ldots, 2^n - 1$. a) Depicts the *PT* distribution for a $\epsilon = 0.012$. The distribution is shown in both liner and logarithmic scale (see inset) and display a heavy-tailed distribution that can be fitted with a power-law curve. This distribution resembles very much to the one presented in Fig. 2.**c**), where the presence of large degree hubs would indicate a scale-free feature of the complex network. b) Shows the *PT* distribution for a $\epsilon = 0.1$. This distribution has the shape of a normal distributions, similar to what was shown in Fig. 2.**f**) for the same value of ϵ.

REFERENCES AND NOTES

1. S. L. Sondhi, S. M. Girvin, J. P. Carini, D. Shahar, Continuous quantum phase transitions. *Rev. Mod. Phys.* **69**, 315–333 (1997).
2. P. W.Higgs Broken symmetries and the masses of gauge bosons. *Phys. Rev. Lett.* **13**, 508–509 (1964).
3. J. Bardeen, L. N. Cooper, J. R. Schrieffer, Theory of superconductivity. *Phys. Rev.* **108**, 1175–1204 (1957).
4. G. M. Luke, Y. Fudamoto, K. M. Kojima, M. I. Larkin, J. Merrin, B. Nachumi, Y. J. Uemura, Y. Maeno, Z. Q. Mao, Y. Mori, H. Nakamura, M. Sigrist, Time-reversal symmetry-breaking superconductivity in Sr_2RuO_4. *Nature* **394**, 558–561 (1998).
5. K. Sacha, J. Zakrzewski, Time crystals: A review. *Rep. Prog. Phys.* **81**, 016401 (2018).
6. F. Wilczek, Quantum time crystals. *Phys. Rev. Lett.* **109**, 160401 (2012.
7. K. Sacha, Modeling spontaneous breaking of time-translation symmetry. *Phys. Rev. A* **91**, 033617 (2015).
8. D. V. Else, B. Bauer, C. Nayak, Floquet time crystals. *Phys. Rev. Lett.* **117**, 090402 (2016).
9. V. Khemani, A. Lazarides, R. Moessner, S. L. Sondhi, Phase structure of driven quantum systems. *Phys. Rev. Lett.* **116**, 250401 (2016).
10. J Zhang, P. W. Hess, A. Kyprianidis, P. Becker, A. Lee, J. Smith, G. Pagano, I.-D. Potirniche, A. C. Potter, A. Vishwanath, N. Y. Yao, C. Monroe, Observation of a discrete time crystal. *Nature* **543**, 217–220 (2017).
11. S. Choi, J. Choi, R. Landig, G. Kucsko, H. Zhou, J. Isoya, F. Jelezko, S. Onoda, H. Sumiya, V. Khemani, C. von Keyserlingk, N. Y. Yao, E. Demler, M. D. Lukin,Observation of discrete time-crystalline order in a disordered dipolar many-body system. *Nature* **543**221–225 (2017).
12. J. Rovny, R. L. Blum, S. E. Barrett, Observation of discrete-time-crystal signatures in an ordered dipolar many-body system. *Phys. Rev. Lett.* **120**, 180603 (2018).
13. J. Smits, L. Liao, H. T. C. Stoof, P. van der Straten, Observation of a space-time crystal in a superfluid quantum gas. *Phys. Rev. Lett.* **121**, 185301 (2018).
14. S. Pal, N. Nishad, T. S. Mahesh, G. J. Sreejith, Temporal order in periodically driven spins in star-shaped clusters. *Phys. Rev. Lett.* **120**, 180602 (2018).
15. N. Y. Yao, A. C. Potter, I.-D. Potirniche, A. Vishwanath, Discrete time crystals: Rigidity, criticality, and realizations. *Phys. Rev. Lett.* **118**, 030401 (2017).
16. K. Giergiel, A. Kosior, P. Hannaford, K. Sacha. Time crystals: Analysis of experimental conditions. *Phys. Rev. A* **98**, 013613 (2018).
17. A.-L. Barabási, R. Albert, Emergence of scaling in random networks. *Science* **286**509–512 (1999.

18. R. Albert, A.-L. Barabási, Statistical mechanics of complex networks. *Rev. Mod. Phys.* **74**, 47–97 (2002.
19. S. Yong, W. Xiangming, Z. Zhenmin, L. Yuan, Using complex network theory in the internet engineering, in *7th Internation Confernce on Computer Science & Education (ICCSE)* (Melbourne, VIC, Australia, 14 to 17 July 2012), pp. 390–394.
20. S. N. Dorogovtsev, J. F. F. Mendes, *Evolution of Networks: From Biological Nets to the Internet and WWW (Physics)* (Oxford Univ. Press, 2003).
21. M. Grifoni, P. Hänggi, Driven quantum tunneling. *Phys. Rep.* **304**, 229–354 (1998).
22. M. Bukov, L. D'Alessio, A. Polkovnikov, Universal high-frequency behavior of periodically driven systems: From dynamical stabilization to floquet engineering. *Adv. Phys.* **64**, 139–226 (2015).
23. A. Eckardt, E. Anisimovas, High-frequency approximation for periodically driven quantum systems from a floquet-space perspective. *New J. Phys.* **17**, 093039 (2015).
24. S. Restrepo, J. Cerrillo, V. M. Bastidas, D. G. Angelakis, T. Brandes. Driven open quantum systems and floquet stroboscopic dynamics. *Phys. Rev. Lett.* **117**, 250401 (2016).
25. A. Eckardt, *Colloquium*: Atomic quantum gases in periodically driven optical lattices. *Rev. Mod. Phys.* **89**, 011004 (2017).
26. V. M. Bastidas, B. Renoust, K. Nemoto, W. J. Munro, Ergodic-localized junctions in periodically driven systems. *Phys. Rev. B* **98**, 224307 (2018).
27. S. Roy, J. T. Chalker, D. E. Logan, Percolation in fock space as a proxy for many-body localization. *Phys. Rev. B* **99**, 104206 (2019).
28. A. C. Potter, R. Vasseur, S. A. Parameswaran, Universal properties of many-body delocalization transitions. *Phys. Rev. X* **5**, 031033 (2015).
29. V. F. Lazutkin. KAM Theorems, in *KAM Theory and Semiclassical Approximations to Eigenfunctions* (Springer Berlin Heidelberg, 1993), pp. 121–159.
30. A. Clauset, C. Shalizi, M. Newman, Power-law distributions in empirical data. *SIAM Rev.* **51**, 661–703 (2009).
31. M. Faccin, T. Johnson, J. Biamonte, S. Kais, P. Migdał, Degree distribution in quantum walks on complex networks. *Phys. Rev. X* **3**, 041007 (2013).
32. G. D. Paparo, M. Müller, F. Comellas, M. A. Martin-Delgado, Quantum google in a complex network. *Sci. Rep.* **3**, 2773 (2013).
33. M. Faccin, P. Migdał, T. H. Johnson, V. Bergholm, J. D. Biamonte, Community detection in quantum complex networks. *Phys. Rev. X* **4**, 041012 (2014).

34. P. W. Anderson, Absence of diffusion in certain random lattices. *Phys. Rev.*, **109**, 1492–1505 (1958).
35. M. Abramowitz, I. A. Stegun, R. H. Romer, Handbook of mathematical functions with formulas, graphs, and mathematical tables. *Am. J. Phys.* **56**, 958 (1988).
36. M. Srednicki, Chaos and quantum thermalization. *Phys. Rev. E* **50**, 888–901 (1994).
37. L. D'Alessio, Y. Kafri, A. Polkovnikov, M. Rigol, From quantum chaos and eigenstate thermalization to statistical mechanics and thermodynamics. *Adv. Phys.* **65**, 239–362 (2016).
38. R. Nandkishore, D. A. Huse, Many-body localization and thermalization in quantum statistical mechanics. *Annu. Rev. Condens. Matter Phys.* **6**, 15–38 (2015).
39. E. Altman, R. Vosk, Universal dynamics and renormalization in many-body-localized systems. *Annu. Rev. Condens. Matter Phys.* **6**, 383–409 (2015).
40. V. Khemani, S. P. Lim, D. N. Sheng, D. A. Huse, Critical properties of the many-body localization transition. *Phys. Rev. X* **7**, 021013 (2017).
41. P. Roushan, C. Neill, J. Tangpanitanon, V. M. Bastidas, A. Megrant, R. Barends, Y. Chen, Z. Chen, B. Chiaro, A. Dunsworth, A. Fowler, B. Foxen, M. Giustina, E. Jeffrey, J. Kelly, E. Lucero, J. Mutus, M. Neeley, C. Quintana, D. Sank, A. Vainsencher, J. Wenner, T. White, H. Neven, D. G. Angelakis, J. Martinis, Spectroscopic signatures of localization with interacting photons in superconducting qubits. *Science* **358**, 1175–1179 (2017).
42. L. D'Alessio, M. Rigol, Long-time behavior of isolated periodically driven interacting lattice systems. *Phys. Rev. X* **4**, 041048 (2014).
43. J. Tangpanitanon, S. Thanasilp, M.-A. Lemonde, D. G. Angelakis, *Quantum Supremacy with Analog Quantum Processors for Material Science and Machine Learning*. arXiv:1906.03860 (2019).
44. G. Engelhardt, V. M. Bastidas, C. Emary, T. Brandes, ac-driven quantum phase transition in the lipkin-meshkov-glick model. *Phys. Rev. E* **87**, 052110 (2013).
45. M. Gong, M.-C. Chen, Y. Zheng, S. Wang, C. Zha, H. Deng, Z. Yan, H. Rong, Y. Wu, S. Li, F. Chen, Y. Zhao, F. Liang, J. Lin, Y. Xu, C. Guo, L. Sun, A. D. Castellano, H. Wang, C. Peng, C.-Y. Lu, X. Zhu, J.-W. Pan, Genuine 12-qubit entanglement on a superconducting quantum processor. *Phys. Rev. Lett.* **122**, 110501 (2019).